Available online at www.sciencedirect.com
SCIENCE DIRECT®
Journal of Sound and Vibration 290 (2006) 448–464
JOURNAL OF SOUND AND VIBRATION
www.elsevier.com/locate/jsvi

Dynamics of 2-dof regenerative chatter during turning

N.K. Chandiramani*, T. Pothala

Department of Mechanical Engineering, Indian Institute of Technology, Guwahati 781039, India

Received 11 June 2004; received in revised form 11 January 2005; accepted 4 April 2005
Available online 14 July 2005

Abstract

A two-degree-of-freedom (2-dof) model comprising nonlinear delay differential equations (DDEs) is analyzed for self-excited oscillations during orthogonal turning. The model includes multiple time delays, possibility of tool leaving cut, additional process damping (due to flank interference), ploughing force, and variations in shear angle and friction angle. Assuming a two-period delay at most, an algorithm based on an existing shooting method for DDEs is developed to simulate tool dynamics and seek periodic solutions. The multiple-regenerative and tool-leaving-cut effects for 2-dof chatter are simulated via an equivalent 1-dof analysis by introducing a time shift. Thus, the cut profile and instantaneous chip thickness are obtained by accounting for chatter motions along both axes. While the amplitude and minimum period of limit cycles computed via shooting and via direct numerical integration compare well, the shooting method converges much faster. Numerical studies involving machining parameters reveal period-1 motion only, for the range of cutting parameters considered here. The possibility of subcritical instability, characterized by the sudden onset of finite-amplitude chatter, is displayed. Additional process damping causes a reduction in chatter amplitudes as well as the subcritical instability to occur at a larger width of cut. An increase in the width of cut causes frequent tool-leaving-cut events and increased chatter amplitudes. The frequency of tool disengagement increases with cutting velocity, despite cutting force in the shank direction remaining constant over a certain velocity range. The chatter amplitude increases and then decreases when the cutting velocity or the uncut chip thickness is increased. The present plant model and dynamics would be useful for state estimator design in active control of tool chatter.

*Corresponding author. Tel.: +91 361 2582653; fax: +91 361 2690762.
E-mail address: naresh@iitg.ernet.in (N.K. Chandiramani).

0022-460X/$ - see front matter © 2005 Elsevier Ltd. All rights reserved.
doi:10.1016/j.jsv.2005.04.012

Nomenclature

V, t_1, w cutting speed, uncut chip thickness, width of cut
T time for one work revolution
$(x, y), (x_0, y_0)$ present-pass chatter displacement, previous-cut profile (Fig. 1)
x_{nT} nth-previous pass chatter displacement of tool
$\phi, \alpha, \gamma, \lambda$ shear, rake, clearance, friction angle
η angle between the x-axis and normal to the machined surface
$()^*$, $\tilde{()}$, $()_e$ solution sought lying on limit cycle, perturbed quantity/computed solution, chatter-free evaluation of quantity
$(\Delta\phi)_B$ variation in shear angle due to tool vibration
$(\Delta\phi)_A$ variation in shear angle due to waviness of previous cut
μ friction coefficient between chip and rake
μ_c friction coefficient between tool nose and displaced work
ψ tool penetration depth
$\mathbf{V}_{W/T}, \mathbf{V}_{C/T}$ relative velocity between—work and tool, chip and tool
$\mathbf{e}_x$, $\mathbf{e}_y$ unit vectors along shank, cutting velocity direction
$\mathbf{n}$ unit vector normal to shear plane
c_x, c_y chatter-free structural and cutting process damping coefficients
μ_x, μ_y additional cutting process damping coefficients
h_x, h_y total damping coefficients
$(F_C, F_T), (F_x, F_y)$ cutting and thrust forces, cutting force components
f_x, f_y ploughing force components
f_{sp}, V_{dm} specific ploughing force, volume of displaced work
τ_s ultimate shear strength
$\mathbf{X}[t], \mathbf{F}, F_l^{(i)}$ state vector, forcing vector, discretization of forcing vector
τ time delay
t, t^* time, shifted time
$P_1[t^*]$, $\mathbf{P}[t^*]$ present-displacement profile, corresponding state vector
$X_{0_1}[t^*]$, $\mathbf{X}_0[t^*]$ previous-cut profile, corresponding state vector
δ, ε small tolerances
$\mathbf{\Phi}[t], \phi_l^{(i)}, \Delta\mathbf{\Phi}^{(i+1)}$ initial-function vector, its discretized components, its correction after ith iteration
$\mathscr{T}^{(i)}$ computed limit cycle period after ith iteration
$\Delta\mathscr{T}^{(i+1)}$ computed correction to limit cycle period after ith iteration
$\mathbf{X}_{\mathscr{T}}, x_{\mathscr{T}_l}^{(i)}$ computed state vector over $[\mathscr{T} - 2T, \mathscr{T}]$, its discretization
$\mathbf{r}^{(i)}$, $z^{(i)}$ computed residual vector, auxillary quantity after ith iteration
$\mathbf{S}^{(i)}$, $\mathbf{g}^{(i)}$ computed variation of state vector with initial function, period
$\mathbf{c}^{(i)}$, $d^{(i)}$ computed variation of auxillary quantity with initial function, period
$S_{ml}^{(i)}$, $g_l^{(i)}$, $c_l^{(i)}$ discretizations of $\mathbf{S}^{(i)}$, $\mathbf{g}^{(i)}$, $\mathbf{c}^{(i)}$

1. Introduction

Self-excited vibrations that occur during machining are termed chatter. Chatter degrades surface finish and causes tool breakage. Passive control of chatter involves limiting the cutting parameters (like width and depth of cut), which in turn limits productivity.

A pioneering stability analysis of 1-dof regenerative chatter, along the shank or the cutting-velocity directions, was done by Tobias and Fishwick [1]. They considered the cutting force to be dependent on the instantaneous chip thickness, and the feed velocity. Ota and Kono [2] considered the effects of delay terms arising due to the cutting force dependency on the

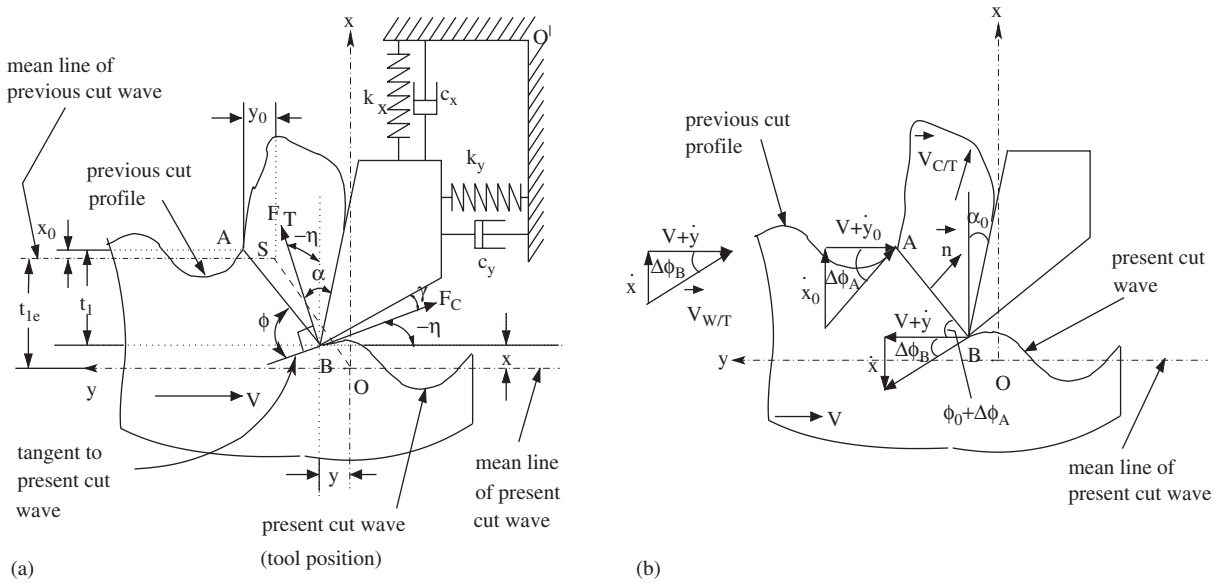

Fig. 1. (a) Cutting tool system and coordinates and (b) kinematics for shear angle [18] and $V_{C/T}$ [9].

instantaneous chip thickness, which in turn depends on the previous cut profile. Hanna and Tobias [3] modeled the machine–tool structure with nonlinear stiffness and hysteretic damping, and the cutting force as a cubic polynomial in chip-thickness-variation (yielding nonlinear delay terms). Their analysis explained experimentally observed 'finite amplitude instability' as occurring as a result of a nearly subcritical instability in the amplitude versus width-of-cut plane (see also Ref. [4]).

Wu and Liu [5] considered a 2-dof system with velocity-dependent friction and an empirical ploughing force. Besides experimental verification, their work showed that chip–rake friction caused chatter whereas interference between tool nose and work-limited chatter. Berger et al. [6] used this model and obtained chaotic/aperiodic and limit-cycle dynamics during small and large amplitude chatter, respectively. Similar prechatter dynamics were experimentally confirmed by Johnson and Moon [7], who also presented a 1-dof DDE model. Moon [8] considered velocity-dependent friction and reported a loss of stability with increasing depth of cut, leading to chatter in the form of quasi-periodic tool motion. Nosyreva and Molinari [9] considered velocity-dependent friction and ploughing force. Their multiple-scales analysis revealed saturation followed by reduction of amplitudes, in accord with experiments.

The 2-dof model of Tlusty and Ismail [10] revealed that tool leaving cut improves stability. Nonlinearities due to tool leaving cut and due to interference between flank and machined wave (causing additional process damping) were considered by Jemielniak and Widota [11] and Tarng et al. [12]. Ploughing force-related damping, due to rounded tool nose and builtup edge, was modeled by Wu [13] and equivalently by Lee et al. [14] using a neural network.

Stepan [15] introduced an additional (short) regeneration time as the chip moved over the tool cutting edge. This distributes the force along the tool–chip interface, yielding an integro-differential equation for the distributed delay. The model predicted greater stability at high cutting speeds, as observed in experiments. Non-stationary turning was modeled as a non-autonomous

DDE with periodically varying delay by Insperger et al. [16], who obtained, via a semi-discretization method, new kinds of instability lobes related to period doubling. Stepan and Nagy [17] performed a center manifold reduction and obtained a simple formula for technological use in deciding the practical chip width below which chatter is avoided. Their analysis showed the existence and nature of a Hopf bifurcation in regenerative chatter. Using a 2-dof chatter model with multiple delays and shear angle variation, Lin and Weng [18] obtained chaotic chatter at certain widths of cut. Subsequently, Hwang et al. [19] obtained the subcritical bifurcation behavior using the method of multiple scales as well as the numerical method of Jemielniak and Widota [11]. The regions of unconditional stability, conditional stability, periodic solution, and instability were demarcated in the spindle-speed versus width-of-cut parameter plane. Nayfeh et al. [20] also considered perturbation methods to analyze tool chatter. Koren [21] reviewed the work on control of machine tools using servocontrol loops to control individual axes, interpolators that coordinate the motion of axes to track desired contours, and adaptive control of cutting parameters to maximize material removal rates subject to constraints on the cutting force, etc.

Solutions to the nonlinear ODEs that govern chatter may be obtained using perturbation methods that are valid for weak nonlinearity, or other more generally applicable methods such as the harmonic balance-based method or numerical methods including shooting-based methods. Notable amongst the perturbation methods are Lindstedt–Poincare-based methods, the method of Multiple Scales, Generalized Averaging, and the Krylov–Bogoliubov–Mitropolsky technique. Since perturbation methods are applicable to a weakly nonlinear system, they provide reasonable results only in the vicinity of the Hopf bifurcation point as the machining parameter (i.e., the width of cut, or the steady-state uncut chip thickness) is varied. Harmonic Balance-based methods work well for strongly nonlinear systems, i.e., when highly subcritical or supercritical values of machining parameters are considered. However, they assume periodicity and require some intuition regarding the number of participating harmonics and the response period (in case of autonomous systems such as the present one), and the resulting algebraic systems are often difficult to solve. Hence, a numerical integration approach based on shooting is adopted herein.

In order to actively control turning-tool chatter without reducing productivity, a plant model that contains all nonlinearities and effects aiding and countering chatter is required. Hence, in this paper a comprehensive, 2-dof, nonlinear model incorporating multiple regeneration, etc., is studied. The multiple time delay effect for 2-dof chatter is considered via a reduction to an equivalent 1-dof analysis by a shift of time scale. Thus, the cut profile and instantaneous chip thickness are obtained by accounting for x as well as y chatter motions. An efficient shooting-based numerical algorithm for problems with multiple delays is used to solve for limit cycles, by assuming a two-period delay at most.

2. Equations governing chatter

Fig. 1(a) shows the tool-work system. The origin O of the $x-y$ system denotes the equilibrium (i.e., chatter free) position of the tool tip. The origin moves, relative to the work, along the y-axis with a velocity V (i.e., the cutting speed). The tool base, i.e., O', and O have identical motion. Point B and line BA denote the tool tip and the shear plane, respectively. During steady cutting, BA coincides with OS. The displacement of B with respect to O, and that of A with respect to S, is

denoted (x, y) and (x_0, y_0), respectively. Quantities t_1, ϕ, α, γ, and λ denote uncut chip thickness, shear angle, rake angle, clearance angle, and friction angle, respectively, and the corresponding 'e'-subcripted quantity depicts the chatter-free value.

Referring to Fig. 1(a), the instantaneous uncut chip thickness is

$$t_1 = t_{1_e} + x_0[t] - x[t]. \tag{1}$$

The shankwise chatter displacement—as measured from the mean (i.e., chatter-free) line—during the nth-previous pass of the tool is defined as $x_{nT} = x[t - nT]$. Here T is the time for one revolution of work. During large chatter motions the tool could disengage from the work causing the machining forces on the tool tip to disappear. This phenomenon is characterized by $t_1 < 0$. Thus, the cut profile generated by the end of the previous pass is given as

$$x_0 = \min[x_{1T}, t_{1_e} + x_{2T}, 2t_{1_e} + x_{3T}, \ldots]. \tag{2}$$

The multiple regenerative effect is due to this dependence of the chip thickness on the chatter displacements of previous passes (Eqs. (1) and (2)).

The shear angle varies due to the tool vibration and the waviness of the previous-cut surface (Fig. 1(b)). Combining these two effects yields [18]

$$\phi = \phi_e + (\Delta\phi)_B + (\Delta\phi)_A, \tag{3a}$$

$$(\Delta\phi)_B = \tan^{-1}[-\dot{x}/(V + \dot{y})], \quad (\Delta\phi)_A = \tan^{-1}[\dot{x}_0/(V + \dot{y}_0)]. \tag{3b}$$

Steady-state cutting tests provide the variation in the coefficient of friction between chip and rake, i.e., $\mu(\equiv \tan[\lambda])$, as [5]

$$\mu = \mu_0 \exp[-m_\mu V_{C/T}], \tag{4}$$

where coefficients μ_0 and m_μ are experimentally determined from cutting test data obtained under conditions of continuous chip flow. Unlike the Coulomb friction model, this one conforms to experiments where the chip–rake friction coefficient has been observed to decrease with cutting speed. The velocity of work relative to the tool is $\mathbf{V}_{W/T} = -\dot{x}\mathbf{e}_x - (V + \dot{y})\mathbf{e}_y$. Using the continuity—across the shear plane—of the relative velocity components normal to the shear plane [9], i.e., $\mathbf{V}_{W/T}.\mathbf{n} = \mathbf{V}_{C/T}.\mathbf{n}$, the velocity of the chip relative to tool ($V_{C/T}$) is obtained as

$$V_{C/T} = \frac{(V + \dot{y})\sin[\phi_e + (\Delta\phi)_A] - \dot{x}\cos[\phi_e + (\Delta\phi)_A]}{\cos[\phi_e + (\Delta\phi)_A - \alpha_e]}. \tag{5}$$

The chatter-free damping coefficients (c_x, c_y) represent structural and cutting process damping. Additional cutting process damping arises due to the interference of the tool flank with the downward-inclined wavy machined surface [11,12]. Hence, the total damping coefficients are given as

$$h_x = c_x(1 - \mathscr{U}[-\dot{x}]\mu_x\eta/\gamma), \quad h_y = c_y(1 - \mathscr{U}[-\dot{x}]\mu_y\eta/\gamma). \tag{6}$$

Here $\mathscr{U}[\cdot]$ is the unit step function, η is the angle (counterclockwise positive) between the x-axis and the normal to the wavy surface (Fig. 1(a)), and μ_x, μ_y are additional cutting process damping coefficients. Thus, one obtains

$$\eta = \tan^{-1}[\dot{x}/(V + \dot{y})] \quad \text{and} \quad \alpha = \alpha_e - \eta. \tag{7}$$

As is evident, the ratio $-\eta/\gamma$ increases [decreases] as the tool moves down a convex [concave] surface, and hence the additional damping increases [decreases], as expected, due to increasing [decreasing] interference between the flank and machined wave.

Due to slight roundedness of the tool nose and the formation of built-up edge, which increases the effective nose radius, a portion of the work material gets displaced (i.e., extruded) under the tool. Thus a ploughing force (f_x, f_y) is exerted on the tool. Following Ref. [13], the ploughing force components are considered as

$$f_x = f_{\text{sp}} V_{dm} \quad \text{and} \quad f_y = -\mu_c f_x, \tag{8}$$

where

$$V_{dm} = w\left[\frac{V}{V\tan\gamma_e + \dot{x}} - \frac{V^2}{(V\tan\gamma_e + \dot{x})^2}\frac{\tan\gamma_e}{2}\right]\psi^2 \tag{9}$$

is the volume of displaced work. Here f_{sp}, μ_c, ψ, and w denote the specific ploughing force, friction coefficient (assumed constant) between tool nose and displaced work, depth of tool penetration, and width of cut (i.e., chip width measured perpendicular to the $x-y$ plane), respectively.

The cutting force (F_C) and thrust force (F_T) shown in Fig. 1(a) are given by the Merchants Circle relations, i.e.,

$$F_C = \frac{wt_1\tau_s\cos[\lambda-\alpha]}{\sin[\phi]\cos[\phi+\lambda-\alpha]}, \quad F_T = \frac{wt_1\tau_s\sin[\lambda-\alpha]}{\sin[\phi]\cos[\phi+\lambda-\alpha]}, \tag{10}$$

where τ_s is the ultimate shear strength. Considering the cutting, thrust, ploughing, and total damping forces, the equations of motion governing chatter are written as (Fig. 1),

$$m\ddot{x} + h_x\dot{x} + k_x x = (F_x + f_x - (f_x)_e)\mathscr{U}[t_1], \tag{11a}$$

$$m\ddot{y} + h_y\dot{y} + k_y y = (F_y + f_y - (f_y)_e)\mathscr{U}[t_1], \tag{11b}$$

$$F_x = -F_C\sin[\eta] + F_T\cos[\eta] - (F_T)_e, \tag{11c}$$

$$F_y = -F_C\cos[\eta] - F_T\sin[\eta] + (F_C)_e, \tag{11d}$$

where $(\cdot)_e$ denotes chatter-free evaluations (i.e., with $x = \dot{x} = y = \dot{y} = 0$). The cutting force components F_x and F_y are measured relative to the chatter-free state, i.e., they disappear during steady cutting ($\eta = 0^\circ$). These are nonlinear DDEs containing the multiple regenerative effect, which arises due to the dependence of the cutting and thrust forces on the instantaneous chip thickness and is characterized by multiple delay terms (Eqs. (1), (2) and (10)). The tool-leaving-cut effect appears via $\mathscr{U}[t_1]$. The nonlinearity is due to the nonlinear dependence of t_1, ϕ, α, λ, and V_{dm} on the state $(x, y, \dot{x}, \dot{y})$.

3. Numerical solution

Defining the state vector as

$$\mathbf{X}[t] = \{X_1, X_2, X_3, X_4\}^{\mathrm{T}} \equiv \{x, \dot{x}, y, \dot{y}\}^{\mathrm{T}}, \tag{12}$$

the resulting system of DDEs, i.e.,

$$\dot{\mathbf{X}}[t] = \mathbf{F}[t, \mathbf{X}[t], \mathbf{X}[t-\tau]] \quad \text{subject to } \mathbf{X}[t] = \mathbf{\Phi}[t] = \mathbf{0} \quad \text{for } -\tau \leqslant t \leqslant 0 \tag{13}$$

is numerically integrated using the RK-4 method. The delay τ equals nT where integer n is the previous-pass number corresponding to the point $x_0[t]$ on the previous-cut profile (PCP) (Eq. (2)). Integration is performed over $[0, T]$, i.e., over one revolution of workpiece. Fig. 2(a) shows the vector sum of x and y chatter displacements, i.e., the present-displacement profile (PDP) P_1. For a constant cutting speed, the horizontal axis denotes time and, equivalently, the distance along the work circumference. Thus, $x[t] = P_1[t^*]$ where $t^* = t + y/V$ is the shifted time. The approximation of constant y-chatter velocity is tacitly implied in the definition of t^*. Using this time shift, the effect of y-chatter is incorporated into the PDP and consequently into the PCP. The instantaneous chip thickness is calculated using both these profiles (Eq. (1)) and then used to obtain machining forces (Eq. (10)). If $t_1 > 0 [t_1 < 0]$ the tool is inside [outside] the cut and machining forces are non-zero [zero]. A time-step bisection is done to determine the instant when $|t_1| \leqslant \delta$, i.e., when the tool leaves or enters the cut (δ is a small positive tolerance).

In accordance with Eq. (2), at the end of the integration interval $[0, T]$ the PCP is updated (using interpolation) with the state vector—chosen out of the PDP and PCP—that has minimum $X_1[t^*]$. The updated PCP is used (with interpolation), during the next interval of integration, as the initial function ($\mathbf{\Phi}[t]$) and also to obtain t_1. The Poincarè surface, defined as

$$\{(X_1, X_2, X_3, X_4) : X_3 = 0, X_4 > 0\} \tag{14}$$

is obtained, and the relative differences over successive Poincarè surface intersections are computed for X_1, X_2, X_4. If these differences remain below a specified small tolerance for the ith and $(i+m)$th intersection (m is the smallest positive integer for which this holds) then convergence to an m-period limit cycle occurs and the period is the interval between the ith and $(i+m)$th intersection. A trivial fixed point is obtained if the Poincarè intersections remain trivial. Note that the numerical integrations are performed in unshifted time t.

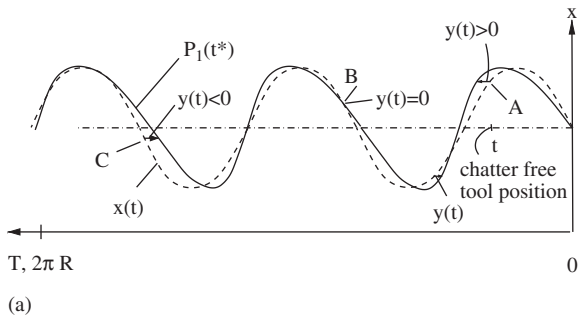

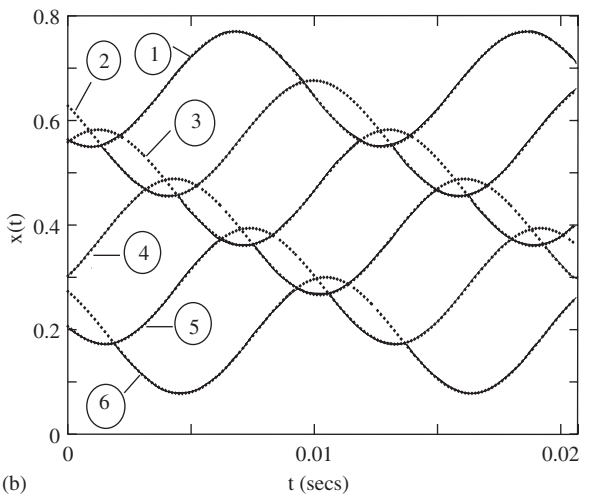

Fig. 2. (a) Time shift and (b) multiple regeneration.

3.1. Direct integration algorithm

Time integration of Eq. (13) is done for a specified number of revolutions, as follows:

[0] Initialize $\mathbf{\Phi}[t]$ (i.e., the intial function) and **Profile** to zero. **Profile** contains t^*, X_1, X_3, X_4, corresponding to PCP.
[1] *Integration over pth pass* $[0, T]$:
Integrate the DDEs (13) over time step $[t_I, t_O]$ to obtain $\mathbf{X}[t_O]$.
Perform time shift $t_O^* \leftarrow t_O + y[t_O]/V$.
Obtain PDP, $\mathbf{P}[t_O^*] \leftarrow \mathbf{X}[t_O]$.
Using interpolation, access **Profile** at t_O^* to extract $\mathbf{X}_0[t_O^*]$, i.e., the state vector corresponding to PCP.
Calculate instantaneous chip thickness (Eq. (1)), $t_1 \leftarrow t_{1_e} + X_{0_1}[t_O^*] - P_1[t_O^*]$.
If t_1 changes sign, i.e., if the tool leaves or enters the cut, perform time-step bisection.
Tooldisp $\leftarrow (t_O^*, \mathbf{P}[t_O^*])$ (here t_O^* pertains to the end of the bisection if it was performed).
[2] *Updating Profile* (Eq. (2)): Using interpolation, **Profile** $\leftarrow (t_O^*, \min_{X_1}(\mathbf{Profile}, \mathbf{Tooldisp}))$.
[3] *Check convergence to limit cycle or fixed point*:
Exit if converged or if the number of tool passes exceeds prescribed limit; else, continue at [1]. If converged to limit cycle then find amplitude and minimum period using Poincarè intersections.

Fig. 2(b) shows the multiple regenerative effect, similar to that reported in Refs. [4,10,11]. Each continuous wave represents the tool displacement profile corresponding to the pass number indicated against it. Solid lines represent the machined surface (cut profile) and the dotted ones indicate tool disengagement. The displacement profile for each pass is shown with respect to the mean-cut (chatter-free) line of that pass. The mean lines of successive passes appear at a distance t_{1_e} below. The tool leaves/enters the cut a multiple number of times during a pass. It is observed that the displacement profile of a pass intersects those of its subsequent two passes only, i.e., the delay is at most $2T$. Hence, in order to implement the following shooting method, $\mathbf{\Phi}[t]$ is assumed to be defined over $[-2T, 0]$.

3.2. Shooting method for periodic solutions

When using direct integration, convergence to a periodic solution is rather slow for parameter values away from the bifurcation point. A zero initial function is considered since the system is assumed to start from rest. However, due to nonlinearity, the speed of convergence would generally also depend on the initial function chosen. Hence, a shooting method is considered to accelerate convergence. This iterative technique uses Newton's method to converge to a periodic solution, if one exists. Following Luzyanina et al. [22] one seeks an initial function, i.e., $\mathbf{\Phi}^*[t]$ defined over $[-2T, 0]$, that lies on the limit cycle, and the period $\mathscr{T}^*$ of the limit cycle. Let $\mathbf{X}_{\mathscr{T}}[\mathbf{\Phi}]$ denote the segment of the solution obtained over $[\mathscr{T} - 2T, \mathscr{T}]$ subject to initial function $\mathbf{\Phi}[t]$. In order to impose the condition that the intial function being sought lies on the limit cycle, we consider the residual equation system that represents this condition, i.e.,

$$\mathbf{r}[\mathbf{\Phi}, \mathscr{T}] \triangleq \mathbf{X}_{\mathscr{T}}[\mathbf{\Phi}] - \mathbf{\Phi} = \mathbf{0}. \tag{15}$$

This system, being indeterminate, is augmented with a suitably chosen auxillary scalar equation, i.e.,

$$z[\mathbf{\Phi}, \mathscr{T}] = 0. \tag{16}$$

An iterative solution of Eqs. (15) and (16) would thus converge to $(\mathbf{\Phi}^*, \mathscr{T}^*)$ if a periodic solution existed. A first-order Taylor's expansion of Eqs. (15) and (16) yields

$$\begin{bmatrix} \mathbf{S}^{(i)} - \mathbf{I} & \mathbf{g}^{(i)} \\ \mathbf{c}^{(i)} & d^{(i)} \end{bmatrix} \begin{Bmatrix} \Delta\mathbf{\Phi}^{(i+1)} \\ \Delta\mathscr{T}^{(i+1)} \end{Bmatrix} = -\begin{Bmatrix} \mathbf{r}[\mathbf{\Phi}^{(i)}, \mathscr{T}^{(i)}] \\ z[\mathbf{\Phi}^{(i)}, \mathscr{T}^{(i)}] \end{Bmatrix}, \tag{17a}$$

where

$$\mathbf{S}^{(i)} \equiv (\partial \mathbf{X}_{\mathscr{T}}/\partial \mathbf{\Phi})^{(i)}, \quad \mathbf{g}^{(i)} \equiv (\partial \mathbf{X}_{\mathscr{T}}/\partial \mathscr{T})^{(i)}, \tag{17b}$$

$$\mathbf{c}^{(i)} \equiv (\partial z/\partial \mathbf{\Phi})^{(i)}, \quad d^{(i)} \equiv (\partial z/\partial \mathscr{T})^{(i)}. \tag{17c}$$

In Eq. (17), the superscript $^{(i)}$ in the coefficient matrix and the driving vector denote evaluations using the solution $(\mathbf{\Phi}^{(i)}, \mathscr{T}^{(i)})$ obtained after the ith iteration. An initial guess $(\mathbf{\Phi}^{(0)}, \mathscr{T}^{(0)})$ of the solution $(\mathbf{\Phi}^*, \mathscr{T}^*)$ is chosen. The algorithm for the $(i+1)$th iteration $(i = 0, 1, 2, \ldots)$ is

[**1**] Integrate the DDEs (13) over $[0, \mathscr{T}^{(i)}]$ subject to initial function $\mathbf{\Phi}^{(i)}$.
[**2**] *Obtain corrections* $(\Delta\mathbf{\Phi}^{(i+1)}, \Delta\mathscr{T}^{(i+1)})$: Evaluate the coefficient matrix (using finite differences) and the driving vector appearing in Eq. (17a) and solve for $(\Delta\mathbf{\Phi}^{(i+1)}, \Delta\mathscr{T}^{(i+1)})$.
[**3**] *Convergence check*: Test whether $\Delta\mathbf{\Phi}^{(i+1)}$ and $\Delta\mathscr{T}^{(i+1)}$ are small relative to $\mathbf{\Phi}^{(i)}$ and $\mathscr{T}^{(i)}$, respectively. If the corrections are relatively small, the converged solution $(\mathbf{\Phi}^*, \mathscr{T}^*) = (\mathbf{\Phi}^{(i)}, \mathscr{T}^{(i)})$ has been obtained (i.e., $\mathbf{X}_{\mathscr{T}}^{(i)} = \mathbf{\Phi}^{(i)}$ and Eq. (15) is satisfied). If not, iterate the solution, i.e.,

$$\mathbf{\Phi}^{(i+1)} = \mathbf{\Phi}^{(i)} + \Delta\mathbf{\Phi}^{(i+1)}, \quad \mathscr{T}^{(i+1)} = \mathscr{T}^{(i)} + \Delta\mathscr{T}^{(i+1)}. \tag{18}$$

Implementation entails discretization of the n-dimensional initial function vector at $(N+1)$ equally spaced time stations within $[-2T, 0]$, i.e.,

$$\mathbf{\Phi}^{(i)} = \{\phi_{11}^{(i)}, \ldots, \phi_{1(N+1)}^{(i)}, \ldots, \phi_{j1}^{(i)}, \ldots, \phi_{jk}^{(i)}, \ldots, \phi_{j(N+1)}^{(i)}, \ldots, \phi_{1(N+1)}^{(i)}, \ldots, \phi_{n(N+1)}^{(i)}\}^{\mathrm{T}}. \tag{19}$$

Step [**1**] is performed using the discretized initial function vector (with interpolation between stations, if required). Using interpolation on the solution vector obtained via integration, the discretized solution vector, i.e.,

$$\mathbf{X}_{\mathscr{T}}^{(i)} = \{x_{\mathscr{T}}{}_{11}^{(i)}, \ldots, x_{\mathscr{T}}{}_{n(N+1)}^{(i)}\}^{\mathrm{T}} \tag{20}$$

is obtained at $(N+1)$ stations lying within $[\mathscr{T}^{(i)} - 2T, \mathscr{T}^{(i)}]$. The discretized residual vector is readily computed using (15), (19), and (20). Introduce the equivalent indexing $l \equiv (j-1)(N+1) + k$, e.g., $\phi_l^{(i)} \equiv \phi_{jk}^{(i)}$. The discretized $n(N+1) \times n(N+1)$ matrix $\mathbf{S}^{(i)}$ is obtained using finite differences. Using the initial function with lth element perturbed by ε, i.e.,

$$\tilde{\mathbf{\Phi}}^{(i)} = \{\phi_1^{(i)}, \ldots, \phi_l^{(i)} + \varepsilon, \ldots, \phi_{(nN+n)}^{(i)}\}^{\mathrm{T}}, \tag{21}$$

the perturbed solution vector, i.e.,

$$\tilde{\mathbf{X}}_{\mathscr{T}}^{(i)} = \{\tilde{x}_{\mathscr{T}1}^{(i)}, \ldots, \tilde{x}_{\mathscr{T}(nN+n)}^{(i)}\}^{\mathrm{T}}, \tag{22}$$

is obtained via integration. Then one computes

$$S_{ml}^{(i)} = (\tilde{x}_{\mathscr{T}m}^{(i)} - x_{\mathscr{T}m}^{(i)})/\varepsilon, \quad m = 1, \ldots, nN+n. \tag{23}$$

Repeating this procedure for $l = 1, \ldots, nN+n$, one obtains $\mathbf{S}^{(i)}$. The discretized $(nN+n)$-dimension vector $\mathbf{g}^{(i)}$ is obtained by perturbing $\tilde{\mathscr{T}}^{(i)} = \mathscr{T}^{(i)} + \varepsilon$ and computing

$$g_l^{(i)} = (x_{\tilde{\mathscr{T}}l}^{(i)} - x_{\mathscr{T}l}^{(i)})/\varepsilon \tag{24}$$

using the unperturbed initial function $\mathbf{\Phi}^{(i)}$.

The discretized auxillary quantity, appearing in Eqs. (16) and (17a), is defined and computed as

$$z^{(i)} \triangleq \sum_{l=1}^{nN+n} F_l^{(i)}(\phi_l^{(i)} - x_{\mathscr{T}l}^{(i)}). \tag{25}$$

Here $F_l^{(i)}$ is the discretized time-derivative of solution $\mathbf{X}_{\mathscr{T}}$ or, equivalently, the discretized driving vector in the state equations (13). The definition in Eq. (25) implies that Eq. (16) is identically satisfied when Eq. (15) is satisfied, i.e., when the solution converges to a limit cycle ($\mathbf{X}_{\mathscr{T}}^{(i)} = \mathbf{\Phi}^{(i)}$). Furthermore, Eqs. (25) and (16) together describe the requirement that the driving vector become normal to the residual vector (defined by Eq. (15)) as convergence is approached. This closely resembles the orthogonality condition proposed by Mees [23] for obtaining periodic solutions of ODEs. The $(nN+n)$ discretized vector $\mathbf{c}^{(i)}$ is computed as

$$c_l^{(i)} = (\tilde{z}^{(i)} - z^{(i)})/\varepsilon, \tag{26}$$

where $\tilde{z}^{(i)}$ is based on $\mathscr{T}^{(i)}$ and $\tilde{\mathbf{\Phi}}^{(i)}$ with its lth element perturbed. Similarly, $d^{(i)}$ is computed as

$$d^{(i)} = (\tilde{z}^{(i)} - z^{(i)})/\varepsilon, \tag{27}$$

where $\tilde{z}^{(i)}$ is based on $\tilde{\mathscr{T}}^{(i)}$ and $\mathbf{\Phi}^{(i)}$. Hence Eq. (17a) represents a system of size $(nN+n+1)$. If $|\Delta\phi_l^{(i+1)}/\phi_l^{(i)}| < \varepsilon$, $l = 1, \ldots, nN+1$, and $|\Delta\mathscr{T}^{(i+1)}/\mathscr{T}^{(i)}| < \varepsilon$ then convergence is achieved. The minimum period is computed based on Poincarè intersections that occur within the converged period $\mathscr{T}^*$.

4. Results and discussion

Unless mentioned otherwise, all effects appearing in the formulation are considered and the shooting method is used with the following data:

Cutting parameters [5,13,14,18]: Dia of work = 25 mm, $t_{1_e} = 0.15$ mm, $w = 4.0$ mm, $V = 200$ m/min, $\alpha_e = 38^\circ$, $m_\mu = 10^{-06}$, $\phi_e = 50.6^\circ$, $\gamma_e = 2^0$, $f_{\mathrm{sp}} = 4.1 \times 10^5$ N/mm^3, $\mu_0 = \mu_c = 0.3$, $\tau_s = 700$ N/mm^2, $\psi = 0.0046$ mm;

Vibration parameters [12]: $m = 40.87$ kg, $c_x = c_y = 19.73$ N s/mm, $\mu_x = 1.464$, $\mu_y = 5.564$, and $k_x = k_y = 180$ kN/m.

Fig. 3(a) shows the transient x-chatter response, obtained via direct integration, for parameter values which make the linearized system unstable. The displacement increases until a steady state (limit cycle) is slowly reached. This follows the trend reported in Ref. [9]. The limit cycle trajectory (in the $\dot{x}-x$, $\dot{y}-y$, and $\dot{y}-\dot{x}$ planes) obtained via both methods (i.e., shooting and direct integration) overlaps (Figs. 3(b) and (c)). The minimum period, x-chatter amplitude, and the number of integration cycles (i.e., work revolutions) until convergence to steady state, are 0.00950141, 0.106324, and 7078, respectively, via direct integration, and 0.00950090, 0.106292, and 1492, respectively, via shooting. An interesting feature is that the $\dot{x}$ and $\dot{y}$ chatter dynamics are nearly in phase, as is evident from the nearly line-like (instead of loop-like) trajectory in Fig. 3(c). The steady-state x-chatter response is shown in Fig. 3(d). Steady-state responses for the additional damping force due to flank interference, and the ploughing force, are shown in Figs. 4(a–c). The additional damping disappears when the tool moves upward along the wavy machined surface (Figs. 3(d) and 4(a)). An increase in width-of-cut causes the ploughing force magnitude to increase and the tool to disengage from work more frequently and for a longer duration (Figs. 4(b) and (c)). Tool disengagement is characterized by the ploughing force suddenly disappearing.

Fig. 5(a) shows the effect of the chatter-free uncut chip thickness on the limit cycle amplitudes obtained for varying widths of cut. At the critical width (i.e., 3.51 mm for $t_{1_e} = 0.5$ mm and 3.64 mm for $t_{1_e} = 0.15$ mm and 0.3 mm) the solution transforms from a fixed point to a limit cycle, i.e., a Hopf bifurcation occurs. For $t_{1_e} = 0.15$ and 0.3 mm a sudden jump to a finite-amplitude

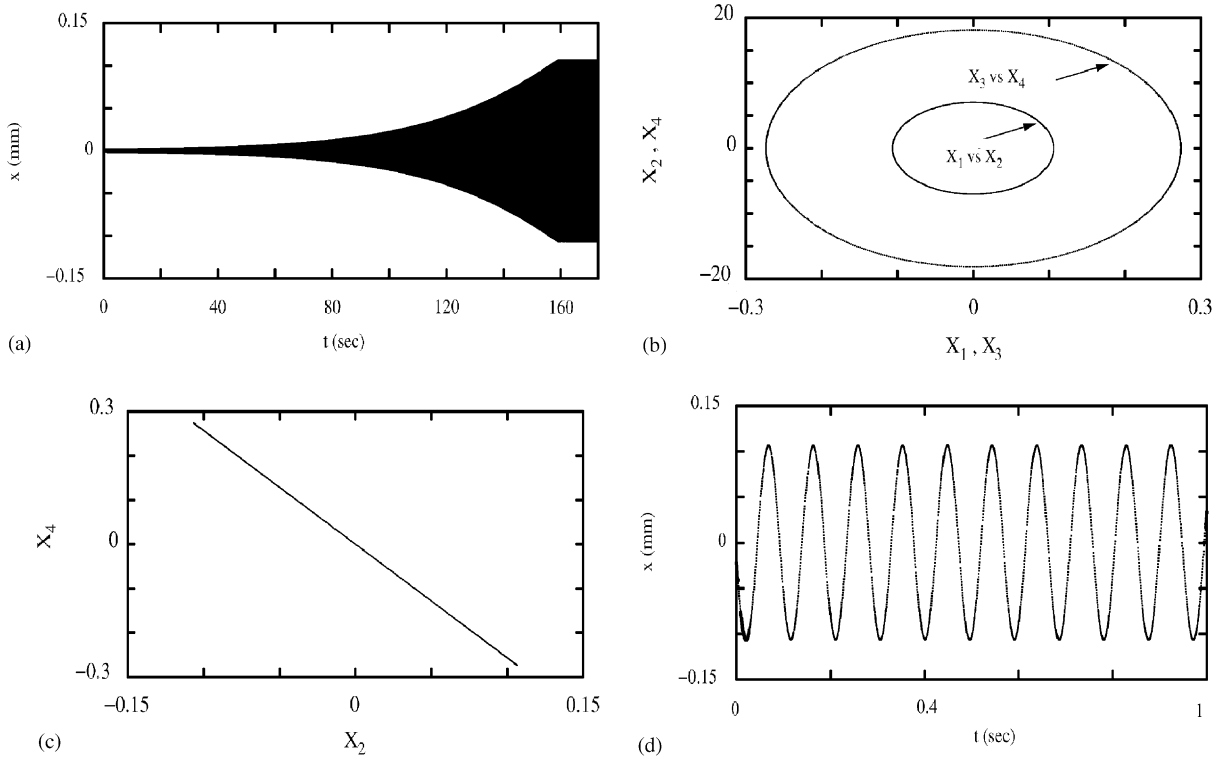

Fig. 3. (a) Transient x-chatter motion, (b,c) limit cycles and (d) steady-state x-chatter motion.

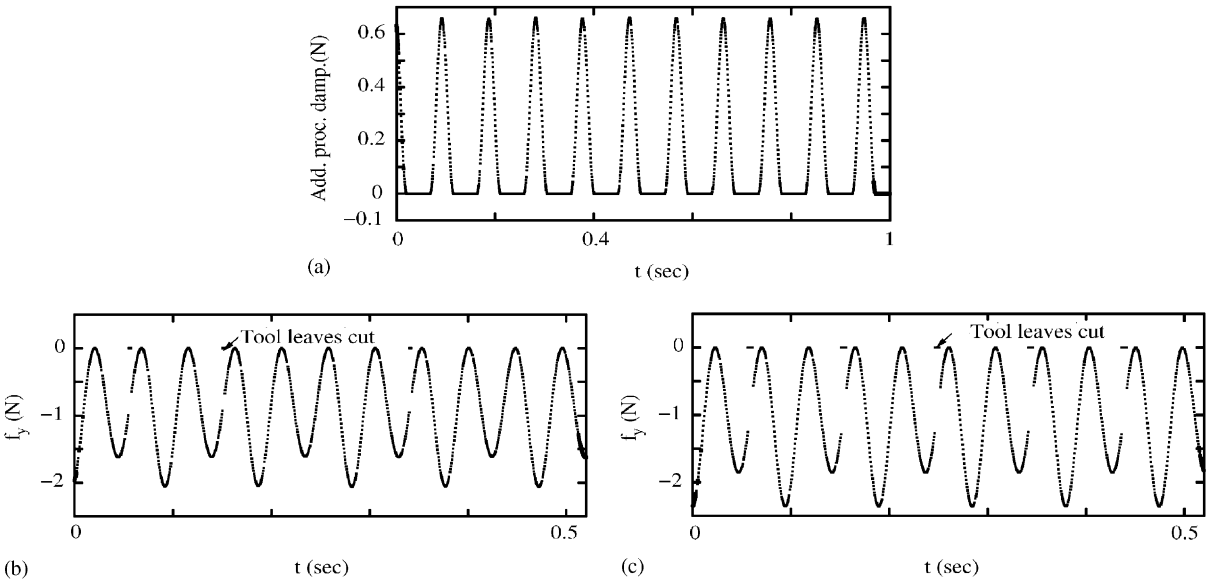

Fig. 4. Steady state: (a) additional process damping force, (b,c) ploughing force—(b) $w = 4$ mm and (c) $w = 4.5$ mm.

limit cycle occurs, thus indicating a subcritical bifurcation. This is qualitatively similar to the results of Refs. [3,4,19]. Hence, for these cases, finite amplitude instability (i.e., pre-chatter motion) is possible for sub-critical widths. As expected, the chatter amplitude increases with uncut chip thickness (since cutting forces increase with t_{1_e}), in accord with the results in Ref. [4]. The direct integration method and the shooting method are compared in Table 1 by means of the number of integration cycles, i.e., work revolutions, required for convergence. The two cases $t_{1_e} = 0.15$ mm and $t_{1_e} = 0.5$ mm of Fig. 5(a) are considered. For $t_{1_e} = 0.5$ mm, i.e., the supercritical case, the number of iterations are comparable for w values chosen close to the bifurcation point. For larger cutting widths (i.e., $w \geqslant 3.85$), the shooting method proves more efficient, the differences becoming more pronounced as the cutting width increases. For $t_{1_e} = 0.15$ mm, i.e., the subcritical case, the shooting method is always more efficient. Thus, when the system starts from rest, the jump to finite-amplitude periodic-chatter involves long-duration transients.

Fig. 5(b) shows the chatter amplitude versus width for cutting velocities 200 and 220 m/min and $t_{1_e} = 0.15$ mm. For a lower cutting speed, the jump occurs for a smaller width and the amplitude is higher. A similar behavior was reported in Ref. [4] when the speed is decreased up to an extent, beyond which the trend reverses. The jump phenomenon disappears for larger uncut chip thickness (i.e., $t_{1_e} = 0.5$ mm, Fig. 5(c)), which is in accord with the results in Ref. [4]. Here also the chatter amplitudes are greater at lower cutting speeds, which follows the behavior reported in Ref. [18] for the supercritical case. An increase in additional process damping coefficients, μ_x and μ_y, results in lower chatter amplitudes as displayed in Fig. 5(d) for $t_{1_e} = 0.5$ mm. A similar increase when $t_{1_e} = 0.15$ mm (Fig. 5(e)) causes the jump to occur at a larger width of cut.

The effect of cutting velocity is shown in Fig. 6(a) for various models. Model 'C' contains all effects, model 'B' neglects ploughing force and friction variation, and model 'A' further neglects flank interference. Model A predicts a decrease in chatter amplitude when the cutting speed is

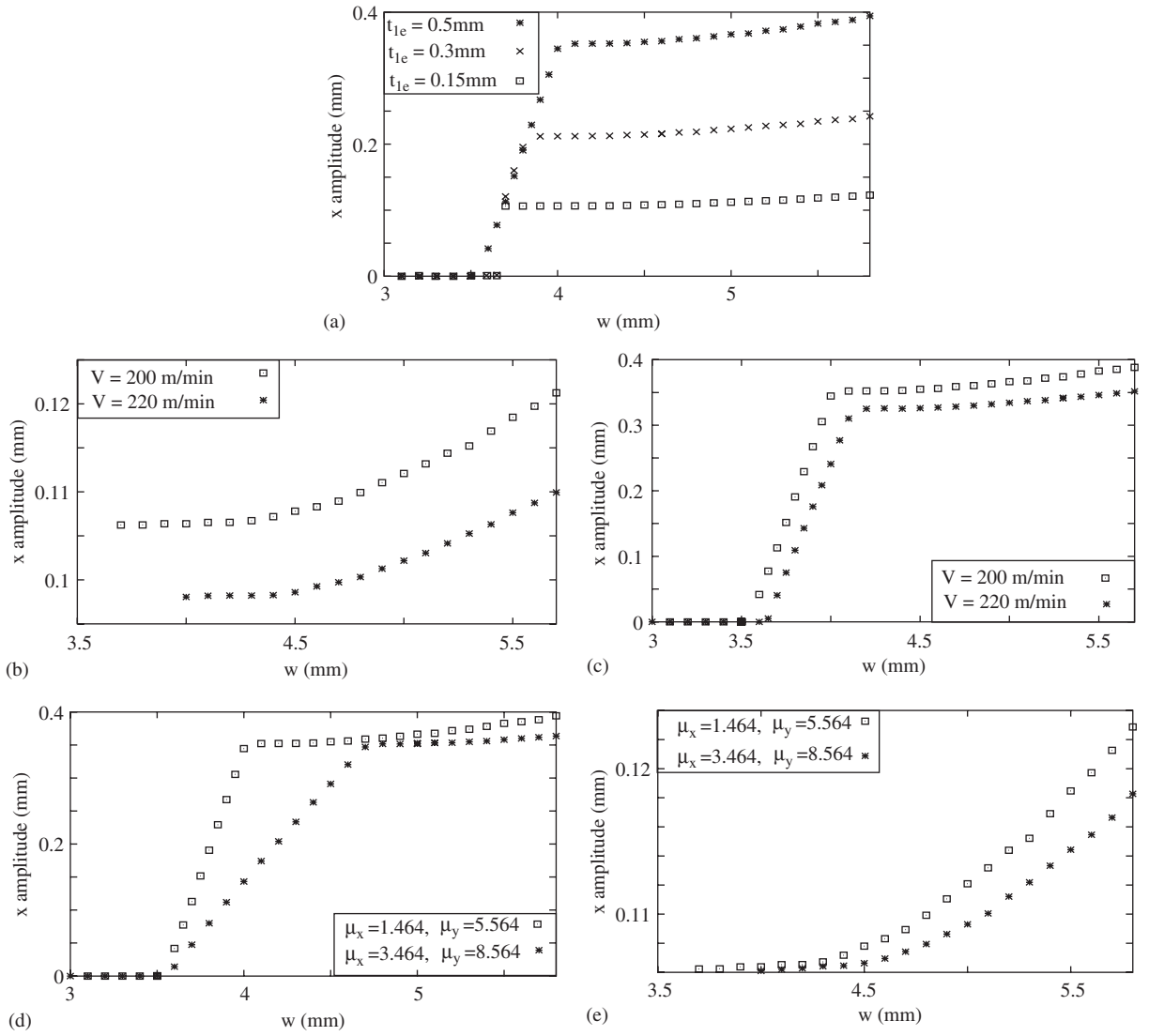

Fig. 5. Chatter amplitude versus width-of-cut, effect of—(a) uncut chip thickness, (b,c) cutting speed, $t_{1_e} = 0.15$, 0.5 mm and (d,e) additional process damping coefficients, $t_{1_e} = 0.5$, 0.15 mm.

increased. When additional process damping is included (model *B*), the amplitude at first increases with cutting speed and then (beyond $V = 130$ m/min) decreases. The amplitudes are lower for the additionally damped system (compare *A* and *B*). A sudden increase in the rate of amplitude reduction occurs at $V = 240$ m/min (model *B*). Further addition of ploughing force and friction variation effects (model *C*) yields a marginal reduction in amplitudes (compare *B* and *C*). A fixed point, i.e., cessation of chatter, occurs beyond $V = 250$ m/min. Fig. 6(b) shows that while the effect of ploughing force is marginal for the value of f_{sp} as considered herein, it generally yields a

Table 1
Comparison of direct integration method and shooting method

$t_{1_e} = 0.15$ mm				$t_{1_e} = 0.5$ mm			
w	x-ampl.	Cycles for convergence		w	x-ampl.	Cycles for convergence	
		Direct	Shooting			Direct	Shooting
3.7	0.106231	7072	1507	3.65	0.077437	173	123
3.8	0.106242	7078	1492	3.70	0.112835	293	151
4.0	0.10638	7086	1643	3.75	0.151722	424	254
4.2	0.106535	7103	1571	3.80	0.190606	738	513
4.4	0.107179	7141	1356	3.85	0.229174	1273	489
4.6	0.108306	7211	1447	3.90	0.267315	1958	493
4.8	0.109922	7245	1779	3.95	0.305435	4097	933
5.0	0.112090	7483	1739	4.00	0.344616	7269	946
5.2	0.114395	7557	1779	4.40	0.353083	8358	1026
5.6	0.119725	8179	1705	4.80	0.360455	8743	966
6.0	0.124951	8497	1885	5.20	0.371783	9873	1074

reduction in chatter amplitude. The variation in chatter amplitude with the chatter-free uncut chip thickness is shown in Fig. 6(c) for $V = 200$ and 220 m/min. It is interesting to note that the trend of monotonically increasing amplitudes is reversed at a higher chip thicknesses. This is in accord with the results in Ref. [18] and in contrast to those reported in Ref. [4] and Fig. 5(a) herein. A similar behavior is obtained for the cutting force amplitude as shown in Fig. 6(d).

Figs. 7(a) and (b) shows the variation of the amplitudes of cutting force components F_x and F_y with the cutting speed, for $w = 4.0$ mm and $t_{1_e} = 0.3$ and 0.5 mm. The force amplitudes along the shank (x) direction are smaller when compared to those along the cutting velocity (y) direction. As expected, the cutting force amplitudes are higher for larger values of chatter-free uncut chip thickness. The amplitudes increase with cutting speed until $V = 90$ m/min for $t_{1_e} = 0.3$ mm, and $V = 115$ m/min for $t_{1_e} = 0.5$ mm. Thereafter, the amplitude remains constant for a wide range of cutting speed. For speeds beyond $V = 230$ m/min the amplitude decreases and eventually becomes zero at $V = 250$ m/min, implying cessation of chatter. The range of speeds for which the cutting force amplitudes remain constant decreases with increase in uncut chip thickness, as also reported in Ref. [14]. Time traces of steady state F_x are shown in Fig. 7(c and d) for $t_{1_e} = 0.5$ mm and speeds $V = 115$ and 230 m/min, i.e., at the start and end of the range for which the amplitudes are constant. The cutting force disappears during tool disengagement, which occurs more frequently at the higher speed despite the cutting force amplitude remaining constant over this range of speeds.

5. Conclusions and scope

A comprehensive 2-dof model of tool dynamics during turning, involving nonlinear DDEs, has been considered. Numerical simulations are done using a shooting method for DDEs and the

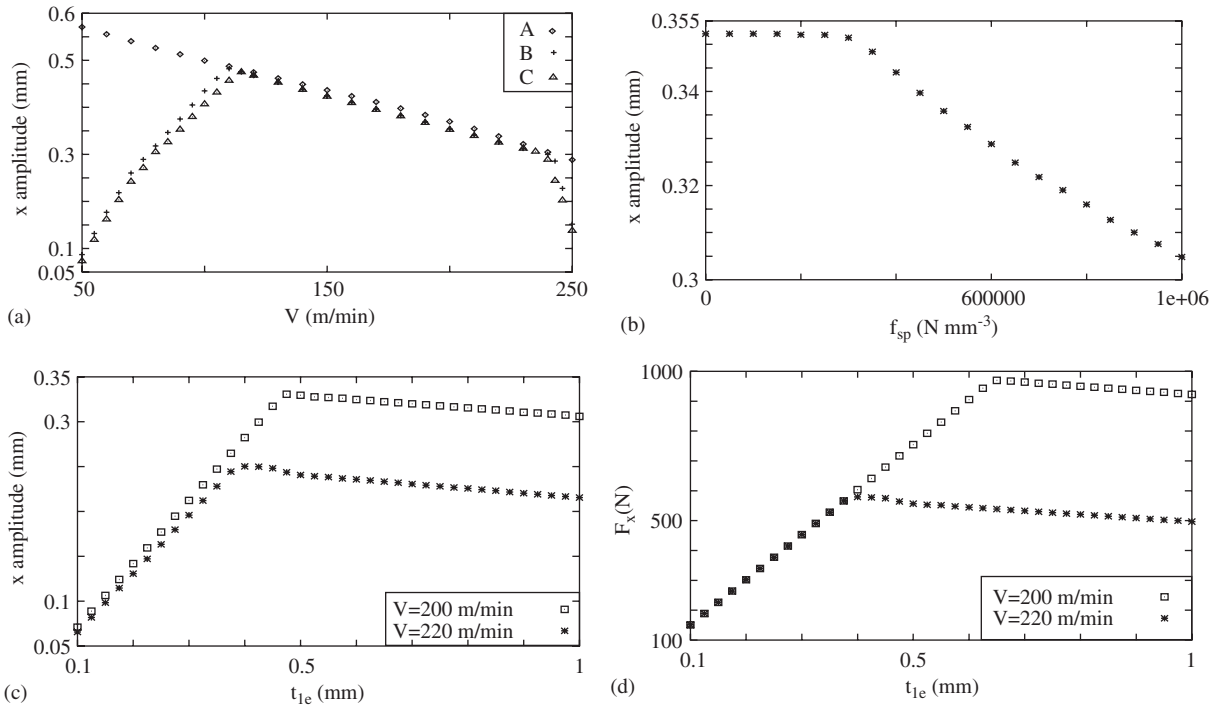

Fig. 6. (a–c) Variation of chatter amplitude with: (a) cutting speed, (b) ploughing force coefficient, (c) uncut chip thickness and (d) cutting force amplitude versus uncut chip thickness.

results compare well with those from direct integration, with the former proving more efficient. Based on the numerical simulations, the following conclusions are made: (i) for the parameter ranges considered, period-1 motion describes the tool dynamics. However, if the stiffness nonlinearity of the machine tool structure were to be considered (as done in Ref. [3]), quasiperiodic as well as chaotic motions may occur for the range of parameters considered herein. (ii) Features of a subcritical Hopf bifurcation could appear in the amplitude versus width-of-cut plane, for certain parameter values. This implies the possibility of subcritical instability characterized by sudden onset of finite-amplitude chatter. (iii) Additional process damping causes a reduction in chatter amplitudes, and the subcritical instability to occur at a larger width of cut. (iv) An increase in width of cut causes frequent tool-leaving-cut events and increased chatter amplitudes. (v) Frequency of tool leaving cut increases with cutting velocity, despite the cutting force in the shank direction remaining constant over a certain velocity range. (vi) The chatter amplitude at first increases and then decreases when the cutting velocity or the uncut chip thickness is increased. (vii) For the parameter ranges considered, variations in friction angle and/or ploughing force have a marginal effect.

The shooting method could be made more efficient using Newton–Picard iterations. Structural nonlinearities, providing a more accurate representation of the machine–tool structure, could be included in the model. Hence, real-time active suppression of chatter could be addressed.

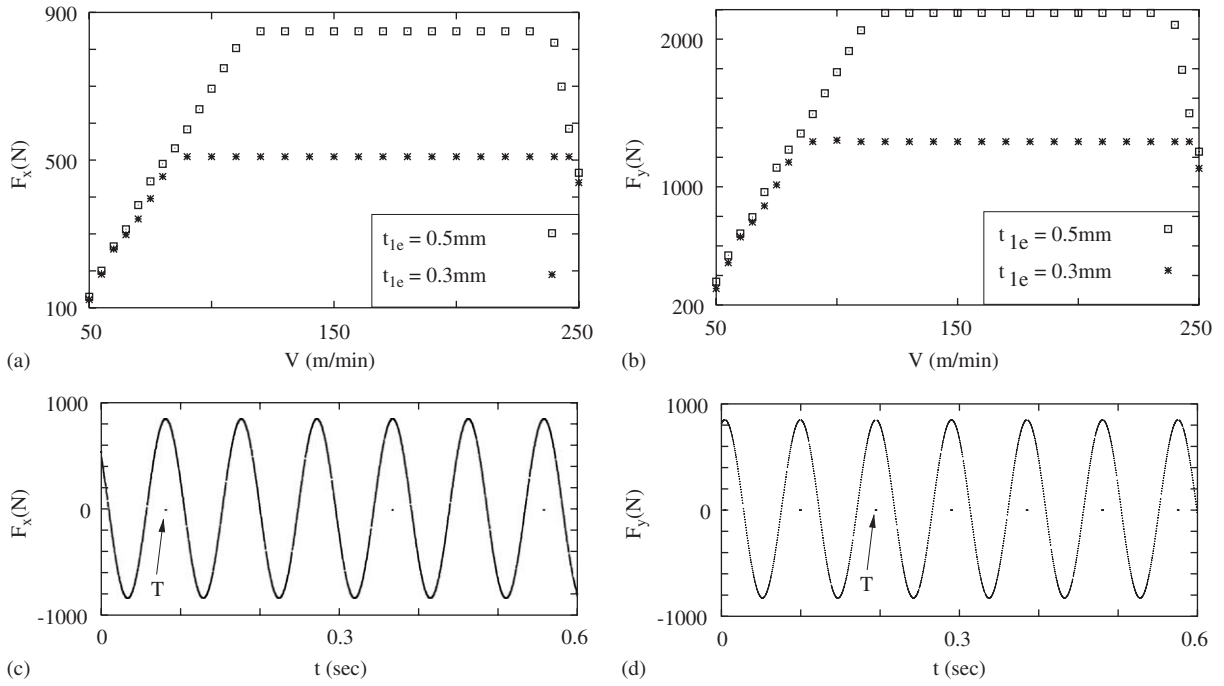

Fig. 7. (a,b) Cutting force amplitude versus velocity, $w = 4.5$ mm, $t_{1_e} = 0.3$, 0.5 mm: (a) F_x, (b) F_y, (c,d) steady-state F_x, $w = 4.5$ mm, $t_{1_e} = 0.5$ mm, 'T' denotes tool leaving cut: (c) $V = 115$ m/min and (d) $V = 230$ m/min.

References

[1] S.A. Tobias, W. Fishwick, The chatter of lathe tools under orthogonal cutting conditions, *Transactions of the American Society of Mechanical Engineers* 80 (1958) 1079–1088.

[2] H. Ota, K. Kono, On chatter vibrations of machine tool or work due to regenerative effect and time lag, *Journal of Engineering for Industry* 96 (1974) 1337–1346.

[3] N.H. Hanna, S.A. Tobias, A theory of nonlinear regenerative chatter, *Journal of Engineering for Industry* 96 (1974) 247–255.

[4] H.M. Shi, S.A. Tobias, Theory of finite amplitude machine tool instability, *International Journal of Machine Tool Design and Research* 24 (1984) 45–69.

[5] D.W. Wu, C.R. Liu, An analytical model of cutting tool dynamics—Part 1: model building—Part 2: verification, *Journal of Engineering for Industry* 107 (1985) 107–118.

[6] B.S. Berger, M. Rokni, I. Minis, The nonlinear dynamics of metal cutting, *International Journal of Engineering Sciences* 30 (1992) 1433–1440.

[7] M.A. Johnson, F.C. Moon, Nonlinear techniques to characterize prechatter and chatter vibrations in the machining of metals, *International Journal of Bifurcation & Chaos* 11 (2) (2001) 449–467.

[8] F.C. Moon, Chaotic dynamics and fractals in material removal processes, in: J.M.T. Thompson, S.R. Bishop (Eds.), *Nonlinearity and Chaos in Engineering Dynamics*, Wiley, Chichester, 1994, pp. 25–37.

[9] E.P. Nosyreva, A. Molinari, Analysis of nonlinear vibrations in metal cutting, *International Journal of Mechanical Sciences* 40 (8) (1998) 735–748.

[10] J. Tlusty, F. Ismail, Basic non-linearity in machining chatter, *CIRP Annals STC C* 30 (1) (1981) 299–304.

[11] K. Jemielniak, A. Widota, Numerical simulation of non-linear chatter vibration in turning, *International Journal of Machine Tools and Manufacturing* 29 (2) (1989) 239–247.

[12] Y.S. Tarng, H.T. Young, B.Y. Lee, An analytical model of chatter vibration in metal cutting, *International Journal of Machine Tools and Manufacturing* 34 (2) (1994) 183–197.
[13] D.W. Wu, A new approach of formulating the transfer function for dynamic cutting processes, *Journal of Engineering for Industry* 111 (1989) 37–47.
[14] B.Y. Lee, Y.S. Tarng, S.C. Ma, Modeling of the process damping force in chatter vibration, *International Journal of Machine Tools and Manufacturing* 35 (7) (1995) 951–962.
[15] G. Stepan, *Retarded Dynamical Systems: Stability and Characteristic Functions*, Pitman Research Notes in Mathematics, Vol. 210, Wiley, New York, 1989.
[16] T. Insperger, G. Stepan, S.N. Namachchivaya, Comparison of the dynamics of low immersion milling and cutting with varying spindle speed, *Proceedings of DETC'01 ASME 2001 Design Engineering Technical Conference and Computers and Information in Engineering Conference*, Paper DETC2001/VIB-21616, Pittsburg, September 9–12, 2001.
[17] G. Stepan, T.K. Nagy, Nonlinear regenerative machine tool vibrations, *Proceedings of DETC'97 ASME 1997 Design Engineering Technical Conference*, Paper DETC97/VIB-4021, Sacramento, September 14–17, 1997.
[18] J.S. Lin, C.I. Weng, Nonlinear dynamics of cutting process, *International Journal of Mechanical Sciences* 33 (8) (1991) 645–657.
[19] C.C. Hwang, R.F. Fung, J.S. Lin, Strong non-linear dynamics of cutting processes, *Journal of Sound and Vibration* 203 (3) (1997) 363–372.
[20] A.H. Nayfeh, C.M. Chin, J. Pratt, Applications of perturbation methods to tool chatter dynamics, in: F.C. Moon (Ed.), *Dynamics and Chaos in Manufacturing Processes*, Wiley Interscience, New York, 1998, pp. 193–214.
[21] Y. Koren, Control of machine tools, *Journal of Manufacturing Science and Engineering* 119 (1997) 749–755.
[22] T. Luzyanina, K. Engelborghs, K. Lust, D. Roose, Computation, continuation and bifurcation analysis of periodic solutions of delay differential equations, *International Journal of Bifurcation and Chaos* 7 (11) (1997) 2547–2560.
[23] A. Mees, *Dynamics of Feedback Systems*, Wiley Interscience, Chichester, 1981.